Two-photon Raman scattering and the polariton dispersion in CdS

H. Schrey, V. G. Lyssenko,* and C. Klingshirn
Institut für Angewandte Physik der Universität, D 7500 Karlsruhe, Federal Republic of Germany

B. Hönerlage
Institut für Theoretische Physik, Universität Regensburg, D 8400 Regensburg, Federal Republic of Germany and Laboratoire de Spectroscopie et d'Optique du Corps Solide (Associé au CNRS N° 232), Université Louis Pasteur, F 67000 Strasbourg, France

(Received 2 August 1979)

Two-photon Raman scattering via virtually excited biexcitons is observed in CdS for different scattering configurations and for different temperatures. A self-consistent evaluation procedure allows one to determine the dispersion curve of the A-exciton polariton. The results are compared to those obtained by other methods, especially resonant Brillouin scattering. Second-order two-photon Raman scattering is reported for the first time.

I. INTRODUCTION

In two-photon Raman scattering (TPRS) or hyper-Raman scattering, a biexciton is created virtually by the coupling of two excitonic polaritons with energy $h\nu_{exc}$ and wave vector $\vec{q}_{exc}$. ($\vec{q}$ refers to wave vectors inside the crystal, whereas those outside the crystal are labeled by a prime.) This biexciton decays into two quasiparticles: One is a polariton $(E_1, \vec{q}_1)$ on the lower branch, which travels to the crystal surface and is detected as a photon $(E_1, \vec{q}_1')$, giving rise to a TPRS line. The other quasiparticle $(E_2, \vec{q}_2)$ is either a longitudinal exciton or an excitonic polariton, or—in uniaxial crystals—a mixed-mode polariton. Throughout the scattering process, energy and momentum of the quasiparticles involved are conserved, since no relaxation takes place in the intermediate state:

$$2h\nu_{exc} = E_1(\vec{q}_1) + E_2(\vec{q}_2)\,, \tag{1}$$

$$2\vec{q}_{exc} = \vec{q}_1 + \vec{q}_2\,. \tag{2}$$

The emission which occurs in this process is of a Raman-type, since its energy changes with the energy of the exciting photons.

The observation of TPRS is of twofold interest. Firstly, it allows the determination of biexciton properties; its symmetry may be deduced from the polarization dependences of exciting and Raman photons,[1,2] and, in some cases, the energetic position of the biexciton ground state may be determined by the TPRS resonance.[2,3] On the other hand, it is possible to reconstruct the dispersion of excitonic polaritons and of longitudinal excitons from TPRS data with great precision. Hereby, energy and momentum conservation [Eqs. (1) and (2)] and the energy-dependent refractive index

$$n[E(\vec{q})] = \frac{c\hbar|\vec{q}|}{E(\vec{q})} \tag{3}$$

are used to calculate the energetic positions of the TPRS emission lines. These energies are compared with the experimental values, and the parameters describing the polariton dispersion $E(\vec{q})$ are then properly adjusted.[4] This study can be carried out at different temperatures.

The procedure described above has first been applied to CuCl and CuBr, crystallizing in T_d symmetry. In these substances, the dispersion relation of excitonic polaritons could be determined quantitatively.[4,5] In this paper we report the application of this method to a uniaxial crystal, namely CdS, belonging to the point group C_{6v}. Here we restrict ourselves to the scattering configuration where the crystallographic $\vec{c}$ axis is perpendicular to the scattering plane (sp); in $\vec{c}$ perpendicular to sp we are dealing with either pure longitudinal excitons or pure transverse polaritons as final-state particles. References to mixed-mode polaritons in the case $\vec{c}$ parallel to sp are given in Refs. 1 and 6.

There exist some other methods to determine the dispersion relation of excitonic polaritons: Reflection and one-photon absorption spectroscopy as well as luminescence measurements are rather indirect ways which involve sophisticated theoretical models, making use of additional boundary conditions, an exciton-free layer, etc. (see, e.g., Refs. 7 and 8). Moreover, absorption spectroscopy near the exciton resonance is possible only for crystals of a thickness $d \simeq K^{-1}$, K being the absorption coefficient. Since $K \geq 10^5$ cm^{-1}, crystals of $d \leq 1$ μm are required.

The evaluation of interference fringes is a more direct method.[9] However, it is possible only in an energetic region away from the exci-

tonic eigenfrequencies, too, because of the importance of the absorption coefficient. Nonresonant two-photon absorption spectroscopy is limited to the upper polariton branch and to the longitudinal exciton because of momentum conservation.[10]

Another direct method to determine the dispersion curve in a rather large region of the first Brillouin zone is resonant Brillouin scattering (RBS).[11] We shall compare our results from TPRS in CdS with those obtained by RBS.

II. EXPERIMENTAL SETUP

The CdS samples are high-quality platelets of a thickness of about 10 μm. They are attached to the copper cold finger of an Oxford evaporation cryostat which allows one to vary the temperature between 5 and 300 K. The two different scattering arrangements used in our study are schematically shown in Fig. 1. In the configuration sketched in Fig. 1(a), the emission from the crystal edge is focused on the entrance slit of the spectrograph. In this case, the internal scattering angle θ between $\vec{q}_1$ and $\vec{q}_2$ is quite large. This configuration is referred to as "backward scattering" in the following. The situation given in Fig. 1(b) corresponds to the forward-scattering geometry. The crystal front surface is excited under an angle of incidence α, and the emission from the rear surface (angle β) is detected.

The excitation source is a N_2-laser-pumped dye-laser in the Hänsch configuration, including a beam-expanding telescope and a grating for wavelength tuning. Using 7D4TMC as the dye, it covers the range of $2.40 \leq h\nu_{exc} \leq 2.70$ eV. The spectral and temporal half-widths of the output pulse are 0.3 meV and 6 nsec, respectively. The electric vector of the exciting light $\vec{E}_{exc}$ is perpendicular to the $\vec{c}$ axis throughout, thus lying in the scattering plane. The TPRS lines are polarized preferentially with $\vec{E}_R$ perpendicular to $\vec{c}$, corresponding to the Γ_1 symmetry of the intermediate biexciton ground state.[1,12-14] In our case, TPRS is observed only when working with rather high excitation intensities I_{exc}; here, 0.2 MW/cm^2 $\leq I_{exc} \leq$ 20 MW/cm^2. As a consequence, the TPRS lines are strongly stimulated and can be observed over a large range of $h\nu_{exc}$ (2.528 eV $\leq h\nu_{exc} \leq$ 2.545 eV), similar to a parametric oscillator, and not only about 1 meV above and below the biexciton resonance.[1,2] The emission spectra are dispersed by a 1-m spectrometer and detected by a SIT vidicon connected to an OMA system.

III. EXPERIMENTAL RESULTS

Let us first present the results for large scattering angles θ [Fig. 1(a)]. Actually, the direction of observation is perpendicular to the exciting beam, imaging the edge of the crystal on the entrance slit of the spectrograph, thus observing the TPRS emission stimulated in the crystal plane and diffused from the crystal edge. Figure 2(a) shows representative emission spectra, taken at different energies $h\nu_{exc}$. Besides the dye-laser Rayleigh-scattered light, one observes the luminescence due to the bound exciton I_1 with its acoustic wing (see, e.g., Ref. 15), and, on the low-energy side, two TPRS lines, R_T and R_L. In Fig. 2(b), the spectral positions E_1 of these lines are displayed as a function of $h\nu_{exc}$. The solid lines are results of the theoretical calculation presented in Sec. IV. They approximately obey Eq. (1) with E_2 being a constant. Numerical values are $E_2 = 2.5516$ and 2.5549 eV for R_T and R_L, respectively.

Figure 3 gives the values of E_2 for the scattering configuration of Fig. 1(a) as a function of the crystal temperature. FE indicates the corresponding variation of the maximum of the free exciton luminescence at low excitation. The three curves exhibit almost an identical variation

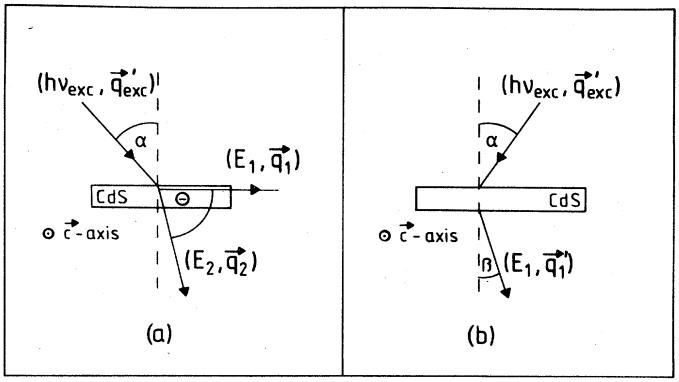

FIG. 1. The geometries used for backward (a) and forward scattering (b). $\vec{q}'$ refers to wave vectors outside the crystal, and $\vec{q}$ to those inside.

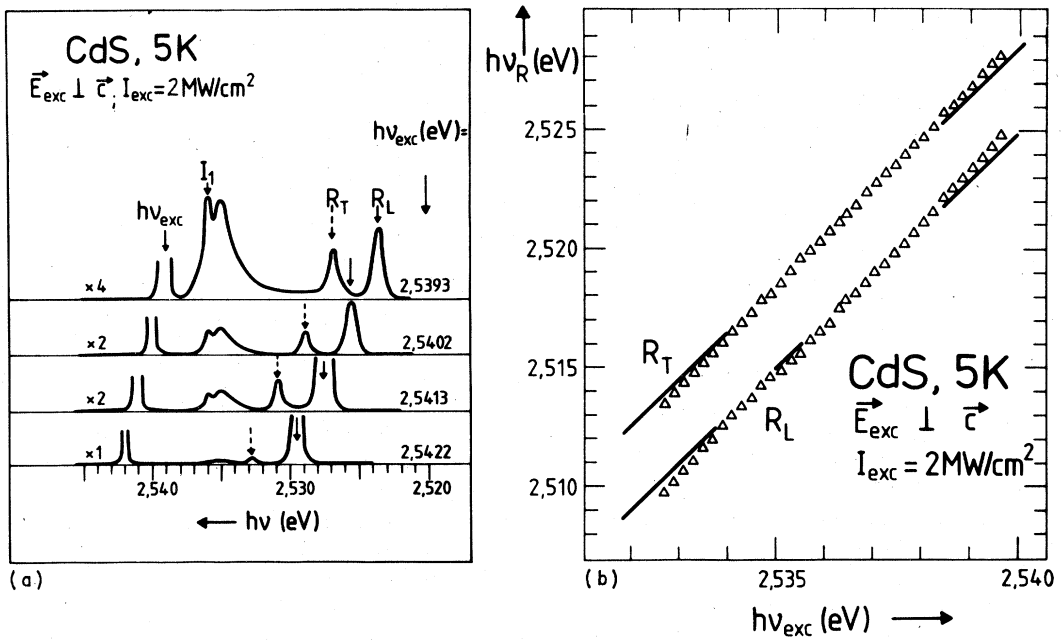

FIG. 2. (a) Emission spectra of CdS at 5 K in the backward scattering configuration n with $\alpha = 40°$ showing the TPRS lines R_T and R_L for different $h\nu_{exc}$. (b) Spectral positions of R_T and R_L as a function of $h\nu_{exc}$; Δ are experimental results; the solid lines, theoretical results.

with temperature.

The forward-scattering results are given in Figs. 4–8. Figure 4 shows emission spectra taken with $\alpha = 12°$ and $\beta = 5°$ for different $h\nu_{exc}$. The diffused light from the dye laser is indicated by arrows. On its high-energy side, the anti-Stokes TPRS emission appears, called R_T^+. The intense lowest-energy peak in each spectrum of Fig. 4 is correspondingly called R_T^-. In addition, two satellites on the high- and low-energy sides of R_T^- are sometimes observed, called R_T^{-+} and R_T^{--}, respectively. Figure 4 shows examples for R_T^{-+}. A satellite R_T^{+-} sometimes occurs between R_T^+

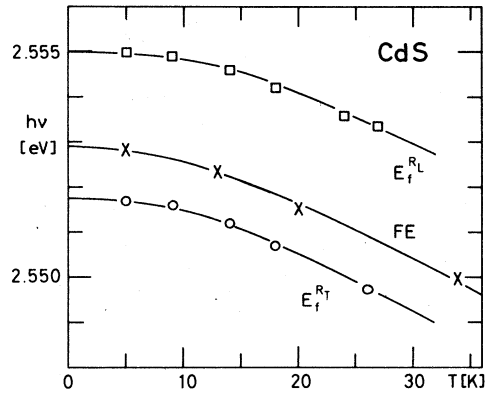

FIG. 3. Temperature dependence of the free-exciton luminescence (FE) and of the final-state energies in TPRS backward scattering.

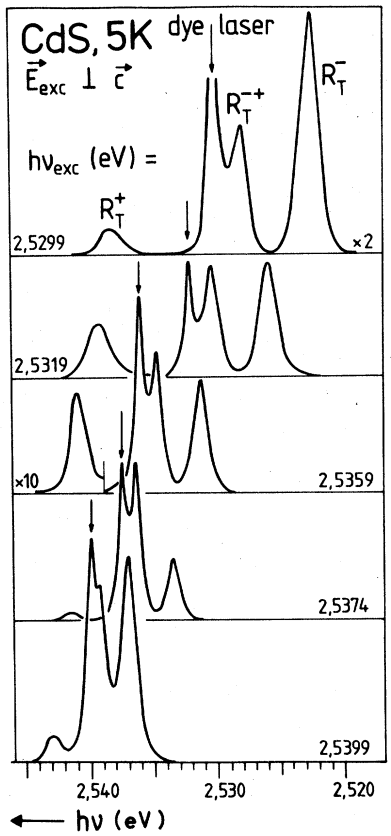

FIG. 4. Emission spectra of CdS at 5 K in the forward-scattering configuration ($\alpha = 12°$, $\beta = 5°$); the parameter is $h\nu_{exc}$.

and $h\nu_{exc}$.

In Fig. 5, the spectral positions of the TPRS lines R_T^+ and R_T^- as a function of $h\nu_{exc}$ are given for different angles of incidence α and fixed direction of observation $\beta = 5°$. In the following, we use the nomenclature (α, β) for describing the forward-scattering geometries. Besides the experimental data, the results of the self-consistent calculation (Sec. IV) are drawn as solid lines.

Examples for the shift of the satellites R_T^{-+} and R_T^{--} with $h\nu_{exc}$ together with the spectral positions of the TPRS lines are shown in Fig. 6 for $\alpha = 12°$ and $\alpha = 57°$. Again, the solid lines are results of the theory. It is noteworthy that the slope of R_T^{--} for $\alpha = 57°$ is larger than 2.

While Figs. 2(b), 5, and 6 show the spectral positions of the TPRS lines as a function of $h\nu_{exc}$ with α as parameter, we display them in Fig. 7 as a function of α for two different $h\nu_{exc}$. The solid lines are again results of the calculation for $(\alpha, 5°)$.

When I_{exc} is raised, the spectral positions of the TPRS lines remain unchanged, whereas their half-widths Γ, as well as those of the dye-laser-scattered light, increase considerably, though the spectral half-width of the incident laser of 0.3 meV remains constant. An example is shown for R_T^- in Fig. 8.

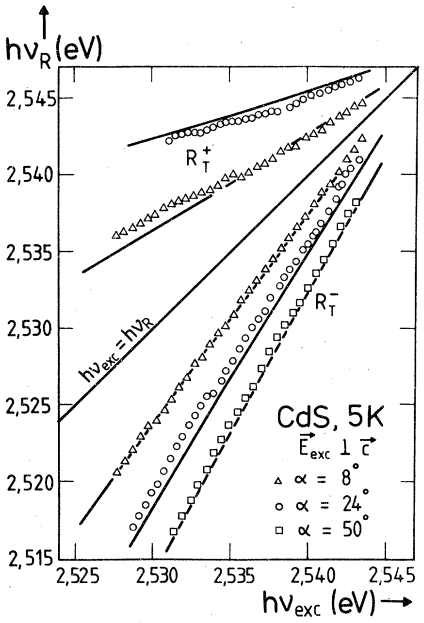

FIG. 5. The spectral positions of the TPRS lines R_T^+ and R_T^- as a function of $h\nu_{exc}$ for different α and fixed $\beta = 5°$. The solid lines are results of the theory.

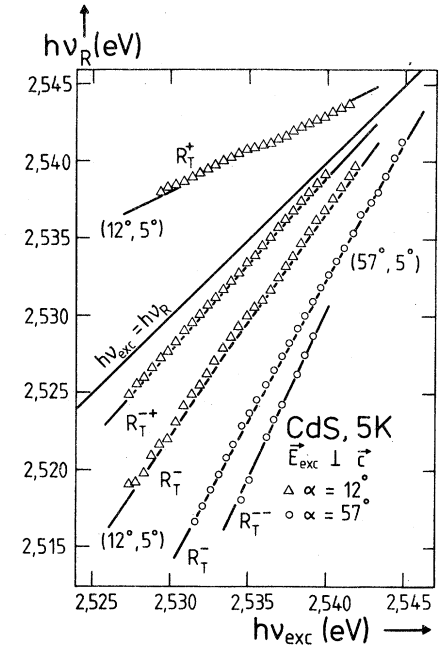

FIG. 6. The spectral positions of the TPRS lines R_T^+ and R_T^- and of the satellites R_T^{-+} and R_T^{--} as a function of $h\nu_{exc}$ for different α and fixed $\beta = 5°$. Solid lines: theory.

IV. THEORETICAL MODEL AND DISCUSSION

As discussed above, the scattering plane is perpendicular to the crystallographic $\vec{c}$ axis

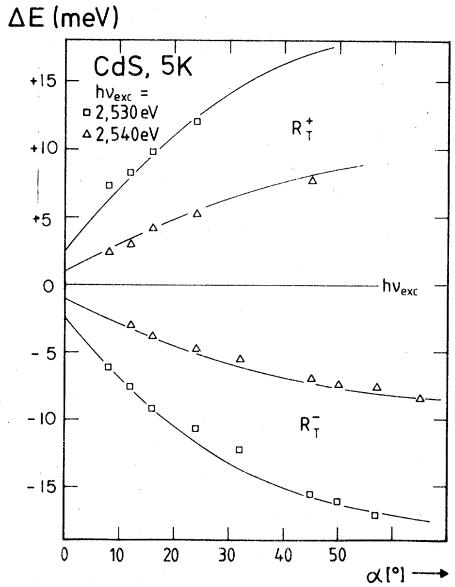

FIG. 7. The spectral positions of the TPRS lines R_T^+ and R_T^- as a function of α for two different values of $h\nu_{exc}$ at fixed $\beta = 5°$. Solid lines: theory.

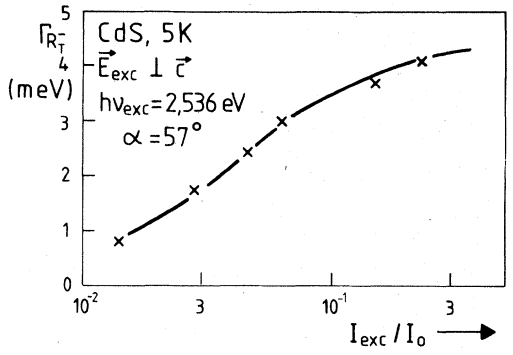

FIG. 8. The half-width Γ (FWHM) of the R_T^- line as a function of I_{exc}. $\alpha = 57°$; $\beta = 5°$; $h\nu_{exc} = 2.536$ eV.

throughout in our experiment. In this configuration, we are studying A excitons; i.e., at $\vec{q}=0$ we are dealing with pure longitudinal exciton states with Γ_5 symmetry ($A^L_{\Gamma_5}$) and with triplet A_{Γ_6} exciton states. The transverse $A^T_{\Gamma_5}$ singlet exciton is coupled to the electromagnetic radiation field, giving rise to a polariton effect. Since the crystal field and the spin-orbit splitting between A and B as well as between A and C exciton states are large compared to the longitudinal-transverse splitting $\Delta_{LT} = E(A^L_{\Gamma_5}) - E(A^T_{\Gamma_5})$, we describe the polariton dispersion in the single-oscillator model of Hopfield[16] and Pekar[17] rather than in the model for interacting resonances, given by Lagois.[18] In this case, the polariton dispersion is simply given by

$$E^{\pm}(\vec{q}) = \frac{1}{\sqrt{2}}\left\{\frac{\hbar^2 c^2 \vec{q}^2}{\epsilon_b} + E_T^2(\vec{q})(1+4\pi\beta^*) \pm \left[\left(\frac{\hbar^2 c^2 \vec{q}^2}{\epsilon_b} + E_T^2(\vec{q})(1+4\pi\beta^*)\right)^2 - \frac{4\hbar^2 c^2 \vec{q}^2}{\epsilon_b} E_T^2(\vec{q})\right]^{1/2}\right\}^{1/2} \tag{4}$$

with

$$E_T(\vec{q}) = E_T + \frac{\hbar^2}{2m_\perp^*}\vec{q}^2 \tag{5}$$

and

$$\frac{\Delta_{LT}}{E_T} = (1+4\pi\beta^*)^{1/2} - 1 \approx 2\pi\beta^*, \tag{6}$$

where $m_\perp^*$ is the effective exciton mass perpendicular to the $\vec{c}$ axis, and ϵ_b is a frequency-independent background dielectric constant. The solutions $E^-(\vec{q})$ and $E^+(\vec{q})$ give the lower and upper polariton branch, respectively. In this model, we have not only neglected the wave-vector-dependent coupling of the A exciton to the other exciton states, discussed in detail by Cho,[19] but also $\vec{q}$-linear interactions between the singlet and triplet states of the A excitons which, however, are generally small. These approximations seem to be justified since the precision of the experiment was not so high as to allow the investigation of warping effects or of the different $\vec{q}$-linear interactions. In addition, if the singlet-triplet interaction is strong, the different exciton states become mixed at finite wave vectors. As discussed in Ref. 5, this mixing becomes apparent in additional TPRS emission lines, which have not been observed in CdS. All these effects can be studied in ZnO, where the A- and B-exciton ground states are close together, and interactions of the different exciton states at finite wave vectors will probably be observed.

Following Goede,[12] the TPRS becomes allowed for transitions to the A_{Γ_5}-exciton states when working with exciting photons with an energy $h\nu_{exc}$ near half the energy of the biexciton with Γ_1 symmetry made up from two A excitons $[AA(\Gamma_1)]$.

This transition has clearly been observed in Fig. 2, where a longitudinal exciton or a lower polariton is left behind and another polariton is observed as a photon. The forbidden transition to a Γ_6 final exciton state does not appear. As discussed in more detail in Ref. 20, the full lines are the result of a self-consistent calculation involving energy and momentum conservation [Eqs. (1) and (2)] and the energy-dependent refractive index $n(\vec{q})$ [Eq. (3)], which is given by the dispersion of the lower polariton branch $E^-(\vec{q})$ [Eq. (4)]. From the different scattering configurations we have determined the following parameters:

$$\begin{aligned} E(A^T_{\Gamma_5}) &= 2.5523 \text{ eV} \pm 0.2 \text{ meV}, \\ \Delta_{LT} &= 2.6 \text{ meV}, \\ \epsilon_b &= 5.4 \pm 0.4. \end{aligned} \tag{7}$$

The effective mass of the exciton, $m_\perp^* = 0.9\, m_0$, was taken from the literature.[21] In our configuration, the TPRS line R_L was not observed in a sufficiently large range in $\vec{q}$ space, so that the curvature of the longitudinal exciton branch could not be determined, in contrast to Refs. 4 and 5.

Figure 9 gives the polariton dispersion curve as calculated with the Hopfield model and using the parameters given above. The crosses in Fig. 9 are corresponding experimental data, where the energy of the observed TPRS emission lines E_1, is attributed to the calculated wave vector $\vec{q}_1$. The energy of the final-state particle not observed in emission, E_2, can be calculated from the experimental data, using energy conservation [Eq. (1)]. The results for values of E_2 and $\vec{q}_2$ are then given by squares in Fig. 9.

Now we are able to explain the origin of the satellite emission lines R_T^{+-}, R_T^{-+}, and R_T^{--}. Since we use platelets with naturally grown plane-parallel surfaces, the TPRS lines R_T^{+} and R_T^{-} are stimulated in this resonator similar to the process described in Ref. 22. Their energies are fixed by the angle of incidence α and by $\beta = 0°$. Due to high I_{exc}, this polariton field is strong enough to initiate a second-order TPRS, which is now observed in our experiment, corresponding to an angular configuration (0°, 5°). Using this model and the parameters given in (7), the calculation yields the solid lines given in Fig. 6 which fit the experimental results for R_T^{-+} and R_T^{--} very well. We have verified the hypothesis of second-order TPRS by pivoting the crystal from $\beta = 5°$ to $\beta = 0°$. In the latter configuration, the satellites R_T^{-+} and R_T^{--} coincide with R_T^{-}.

Concerning the variation with temperature of the final-state energies E_2, displayed in Fig. 3, we note that it is approximately parabolic at low temperatures and almost linear for $T \geq 15$ K. As the variation is nearly identical for R_L and R_T, the L-T split and thus the oscillator strength of the A exciton is constant in this temperature range.

The intrinsic line width Γ of the TPRS emission in forward scattering is governed by the line width and divergence of the exciting photon beam and by the aperture of the spectrograph. With our data, we calculate $\Gamma \approx 1$ meV. The increase of the half-widths of the Rayleigh-scattered dye-laser light and of the TPRS lines with I_{exc} (Fig. 8) is tentatively ascribed to collisions between the polaritons involved in this process. Further investigation has to be carried out to quantitatively understand this observation.

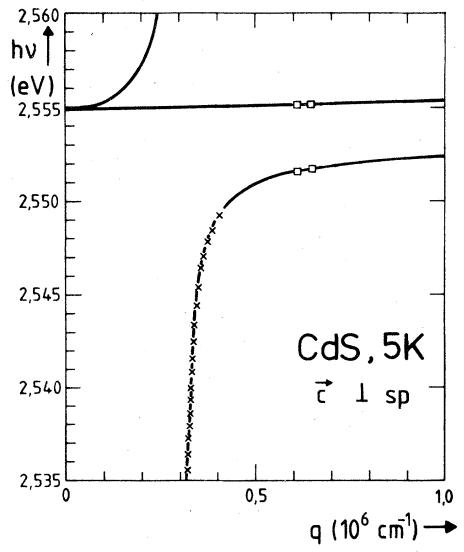

FIG. 9. The dispersion curve of the A_{Γ_5}-polariton in CdS for $\vec{q}$ perpendicular to $\vec{c}$ as deduced from TPRS; × and □ are experimental results for forward and backward scattering, respectively. The theory is given by the solid lines.

V. COMPARISON WITH OTHER RESULTS

Our value of $E(A_{\Gamma_5}^L) = 2.5549$ eV ± 0.2 meV is in good agreement with data recently obtained by the analysis of reflection spectra [2.5548 eV (Ref. 7) and 2.5546 (Ref. 8)] and of interference fringes of extremely thin CdS platelets [2.5547 eV (Ref. 9)]. The energy of the transverse exciton, $E(A_{\Gamma_5}^T) = 2.5523$ eV, as deduced from our experiments, is slightly lower, however; from reflection the values of 2.5527 eV (Ref. 7) and 2.5524 eV (Ref. 8), from interference fringes, 2.5528 eV (Ref. 9) have been obtained. This may be due to the difficulties inherent in the evaluation of these experimental methods, already mentioned in Sec. I, and to additional assumptions such as frequency- and wave-vector-independent damping.

Our value for $E(A_{\Gamma_5}^T) = 2.5523$ eV is slightly below the widely used eigenenergy of the Γ_6 triplet exciton, $E(A_{\Gamma_6}) = 2.5524$ eV[23]. This discrepancy is removed, however, when converting the wavelength in air of Ref. 23 into energy using the refractive index of air [n_{air}(4800 Å) = 1.000 278 6][24] and the appropriate conversion factor (12 398.520 eV Å).[25] This yields the corrected triplet energy $E(A_{\Gamma_6}) = 2.5520$ eV.

Figure 10 gives a comparison of data from RBS[11b] with the dispersion curves obtained with our parameters. Starting with the incident photon energies and the experimentally observed Brillouin shifts in RBS, both taken from Ref. 11b, we calculated the energy and momentum transfer in backward-scattering configuration using the sound velocities given in Ref. 26. Introducing these values into our dispersion curve, one reaches the final states indicated in Fig. 10 for different scattering processes.

In the excitonlike part of the lower branch, the agreement is good, whereas a significant deviation occurs in its photonlike part. For the fit of

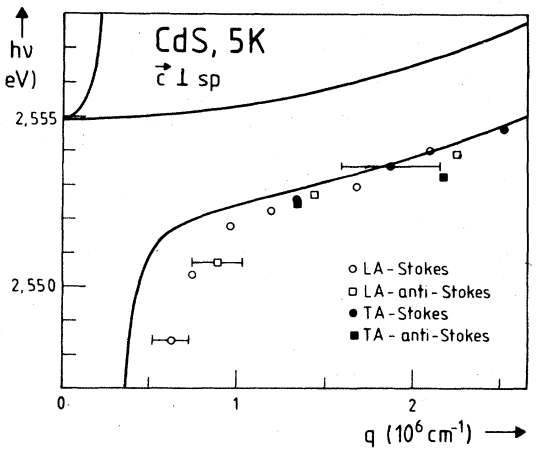

FIG. 10. The A_{Γ_5}-polariton dispersion curve obtained from TPRS (solid line) in comparison with corresponding results from resonant Brillouin scattering (Ref. 11b).

their experimental results these authors[11b] use a background dielectric constant $\epsilon_b = 9.3$. This value is determined about 2 meV below the exciton resonance, and is almost twice the value we deduce from TPRS. In the energetic region near the excitonic bottleneck, the background dielectric constant used in a one-oscillator model differs from the high-frequency dielectric constant ϵ_∞ which has been determined[27] in the Reststrahlen absorption region to $\epsilon_\infty = 5.27$. This difference is due to the contribution of other oscillators which, here, lie close by in energy. For instance, Bruce and Cummins[28] measured RBS about 3...8 meV below the resonance and obtained $\epsilon_b = 8.5$; this is close to the value given by Ref. 11b.

Although we work some 10...30 meV below the resonance, we feel that our value of ϵ_b is too small to be consistent with the results of Refs. 11b and 28. A possible explanation is the deformation of the polariton dispersion due to the high level of excitation in our experiment or to the presence of biexcitons. The discrepancy between RBS and TPRS, however, shown in Fig. 10, might also be due to the fact that both RBS[11,28] and transmission measurements[9] are carried out close to the transverse eigenfrequency where strong one-photon absorption sets in, which is connected with an appreciable imaginary part of the dielectric constant. Damping effects have not been considered in the Hopfield model but are not very important in the TPRS studied here, since the frequencies of exciting and emitted light are far away from the resonance.

VI. CONCLUSION

It has been shown that $\vec{q}$-space spectroscopy by TPRS via virtually excited biexcitons can successfully be applied to uniaxial crystals. By fitting the experimental data, the parameters describing the A excitons in CdS are determined as well as their temperature dependence. Using other scattering geometries, it will be possible to determine the dispersion curves of mixed-mode polaritons by the same method. The experimental determination of their energy in a corresponding TPRS experiment[6] ($E_2^{(\mathrm{exp})} = 2.5538$ eV) is in close agreement with the value calculated with the exciton parameters given here ($E_2^{(\mathrm{theor})} = 2.5539$ eV). Moreover, some hints are obtained on the deformation of the polariton dispersion due to the high excitation.

ACKNOWLEDGMENTS

The authors wish to thank Professor I. Broser, Berlin, Dr. J. B. Grun, Dr. Strasbourg, and Dr. E. S. Koteles, New York, and Professor U. Rössler, Regensburg, for stimulating discussions. This work was supported by the Deutsche Forschungsgemeinschaft.

*Permanent address: Institute of Solid State Physics, Academy of Science of the USSR, Chernogolovka, USSR.

[1] Y. Nozue, T. Itoh, and M. Ueta, J. Phys. Soc. Jpn. 44, 1305 (1978).
[2] H. Schrey and C. Klingshirn, Solid State Commun. 28, 9 (1978) and Phys. Status Solidi B 93, 679 (1979).
[3] T. Itoh, Y. Nozue, and M. Ueta, J. Phys. Soc. Jpn. 40, 1791 (1976).
[4] B. Hönerlage, A. Bivas, and Vu Duy Phach, Phys. Rev. Lett. 41, 49 (1978).
[5] A. Bivas, Vu Duy Phach, B. Hönerlage, U. Rössler, and J. B. Grun, Phys. Rev. B 20, 3442 (1979).
[6] H. Schrey, V. G. Lyssenko, and C. Klingshirn, Solid State Commun. 31, 299 (1979).
[7] W. Stössel and H. J. Wagner, Phys. Status Solidi B 89, 403 (1978).
[8] I. Broser, M. Rosenzweig, R. Broser, M. Richard, and E. Birkicht, Phys. Status Solidi B 90, 77 (1978).
[9] J. Voigt, M. Senoner, and J. Rückmann, Phys. Status Solidi B 75, 213 (1976); J. Voigt, F. Spiegelberg, and M. Senoner, Phys. Status Solidi B 91, 189 (1979).
[10] D. Fröhlich, E. Mohler, and P. Wiesner, Phys. Rev. Lett. 26, 554 (1971).
[11] G. Winterling and E. Koteles, (a) Solid State Commun. 23, 95 (1977); (b) Proceedings of the International Conference on Lattice Dynamics, Paris, 1977, edited by M. Balkanski (Flammarion, Paris, 1978), p. 170; in the conversion of wave numbers into photon energies, the refractive index of air has been taken into account by us.
[12] O. Goede, Phys. Status Solidi B 81, 235 (1977).

[13]F. Henneberger, K. Henneberger, and J. Voigt, Phys. Status Solidi B 83, 439 (1977).
[14]R. Planel and C. Benoît à la Guillaume, Phys. Rev. B 15, 1192 (1977).
[15]J. Shah, R. F. Leheny, and W. F. Brinkman, Phys. Rev. B 10, 659 (1974).
[16]J. J. Hopfield, Phys. Rev. 112, 1955 (1958).
[17]S. J. Pekar, Zh. Eksp. Teor. Fiz. 33, 1022 (1957) [Sov. Phys.—JETP 6, 785 (1958)].
[18]J. Lagois, Phys. Rev. B 16, 1699 (1977).
[19]K. Cho, Phys. Rev. B 14, 4463 (1976).
[20]Vu Duy Phach, A. Bivas, B. Hönerlage, and J. B. Grun, Phys. Status Solidi B 86, 159 (1978).
[21]D. G. Thomas, Phys. Rev. 122, 1 (1961).
[22]R. Levy and J. B. Grun, J. Lum. 5, 406 (1972).
[23]J. J. Hopfield and D. G. Thomas, Phys. Rev. 122, 35 (1961); Phys. Rev. Lett. 15, 22 (1965).
[24]*Handbook of Chemistry and Physics*, 56th ed. (Chemical Rubber Publishing Company, CRC Press, Cleveland, Ohio, 1975/76).
[25]CODATA Bulletin 11, 6 (1973).
[26]D. Gerlich, J. Phys. Chem. Sol. 28, 2575 (1967).
[27]H. W. Verleur and A. S. Barker, Jr., Phys. Rev. 155, 750 (1967).
[28]R. H. Bruce and H. Z. Cummins, Phys. Rev. B 16, 4462 (1977).